Available online at www.sciencedirect.com
SCIENCE DIRECT®
International Journal of Solids and Structures 43 (2006) 1594–1612
INTERNATIONAL JOURNAL OF SOLIDS and STRUCTURES
www.elsevier.com/locate/ijsolstr

An implicit consistent algorithm for the integration of thermoviscoplastic constitutive equations in adiabatic conditions and finite deformations

R. Zaera *, J. Fernández-Sáez

Department of Continuum Mechanics and Structural Analysis, University Carlos III of Madrid, Avda. de la Universidad, 30. 28911 Leganés, Madrid, Spain

Received 25 November 2004; received in revised form 26 March 2005
Available online 31 May 2005

Abstract

The so-called viscoplastic consistency model, proposed by Wang, Sluys and de Borst, is extended here to the integration of a thermoviscoplastic constitutive equation for J_2 plasticity and adiabatic conditions. The consistency condition in this case includes not only strain rate but also the effect of temperature on the yield function. Using the backward Euler integration scheme to integrate the constitutive equations, an implicit algorithm is proposed, leading to generalized expressions of the classical return mapping algorithm for J_2 plasticity, both for the iterative calculation of the plastic multiplier increment and for the consistent tangent operator when strain rate and temperature are considered also as state variables of the hardening equation. The model was implemented in a commercial finite element code and its performance is demonstrated with the numerical simulation of four Taylor impact tests.

Keywords: Finite element solution; Viscoplastic; Thermal softening; Impact; Finite deformation

1. Introduction

Many advanced processes in engineering such as high-speed metal forming (Rojek et al., 2001) and cutting (Molinari et al., 2002; Bäker et al., 2002), structures under crashes (Reyes et al., 2002), high-speed impact on metallic armours (Yadav et al., 2001; Rosenberg et al., 2004) and others, involve complex thermomechanical and multiaxial loading conditions which include large strain, high strain rates,

* Corresponding author. Tel.: +34 916249983; fax: +34 916249430.
E-mail address: rzaera@ing.uc3m.es (R. Zaera).

0020-7683/$ - see front matter © 2005 Elsevier Ltd. All rights reserved.
doi:10.1016/j.ijsolstr.2005.03.070

Notations

c_v	specific heat
C	linear isotropic elastic tensor
d	rate of deformation tensor
F	deformation gradient tensor
l	velocity gradient tensor
r	plastic strain rate direction
s	deviatoric stress tensor
α	coefficient of thermal expansion
$\bar{\varepsilon}^{\mathrm{p}}$	equivalent plastic strain
η	Quinney–Taylor coefficient
ρ	material density
σ	Cauchy stress tensor
$\bar{\sigma}$	equivalent stress
σ_{Y}	yield stress
θ	temperature

temperature softening, adiabatic processes, etc. The numerical simulation of these phenomena requires the integration of the constitutive equations of the material, accounting for thermoviscoplastic hardening relations such as those proposed by Johnson and Cook (1983), Bodner et al. (1975), Zerilli et al. (1987), Litonski (1977) or the more recent equation by Rusinek and Klepaczko (2001). Two major kinds of model can be formulated to account for viscoplastic behaviour of materials: the *overstress models* (such as Perzyna (1966) and Duvaut and Lions (1972)) and the so-called *consistency model*, first proposed by Wang (1997) and Wang et al. (1997) and used by others (Ristinmaa et al., 2000; Winnicki et al., 2001; Heeres, 2001). Using the overstress models, the consistency condition is not fulfilled and stress states outside the yield surface are allowed so the Kuhn–Tucker conditions are not applicable. On the other hand, in the second approach the consistency condition for the yield function is enforced to include rate effects i.e.

$$f(\sigma, \vec{\kappa}, \dot{\vec{\kappa}}) = 0 \quad \text{at } \dot{\lambda} > 0 \tag{1}$$

$\vec{\kappa}$ being a vector including all the state variables and λ the plastic multiplier.

To integrate the set of non-linear thermoviscoplastic constitutive equations into the finite element method, two main tasks must be accomplished at level of the material point. The first one concerns the update of stress and state variables, driven by the strain increment. The second is related to the proper construction of the tangent stiffness used in global implicit FE algorithms, since the quadratic rate of convergence can be preserved only if a consistent (algorithmic) material stiffness is adopted (Simo et al., 1985; Ju, 1990).

In this paper, the consistency model is extended to integrate the thermoviscoplastic constitutive equations for adiabatic conditions and finite deformations. Using the backward Euler scheme, this consistency model provides a fully implicit numerical algorithm similar to the closest point projection commonly used for rate-independent problems on account of their robustness and stability. The update of stress and state variables is achieved through the solution of a single scalar non-linear equation in the plastic multiplier increment $\Delta\lambda$. Then the consistent tangent operator is determined by a systematic linearization of the corresponding algorithm.

The proposed scheme was implemented in the finite element commercial code ABAQUS/Explicit (2003) and its performance is demonstrated through the numerical simulation of four Taylor impact tests.

2. Models for rate-dependent plasticity at small strain

In classical viscoplasticity models, additive decomposition of the strain rate tensor into elastic and plastic parts is assumed

$$\dot{\epsilon} = \dot{\epsilon}^{\mathrm{e}} + \dot{\epsilon}^{\mathrm{p}} \tag{2}$$

where no thermal deformations are considered. If an associated flow rule is adopted, the plastic strain rate tensor is given by

$$\dot{\epsilon}^{\mathrm{p}} = \dot{\lambda}\frac{\partial f}{\partial \sigma} \tag{3}$$

λ being the plastic multiplier defining the magnitude of the plastic flow and f the yield function which depends on stress and state variables. The gradient of f with respect to the stress defines the direction of the plastic flow. Next, two different approaches to define the viscoplastic behaviour of metallic materials are outlined.

2.1. Perzyna overstress model

A widely used viscoplastic formulation is the Perzyna model (Perzyna, 1966) whose main feature is that the yield function can be larger than zero. This effect, known as overstress, is a consequence of the explicit definition of the plastic multiplier

$$\dot{\lambda} = \frac{1}{\kappa}\langle \Phi(f_{\mathrm{P}})\rangle \tag{4}$$

where $\langle\circ\rangle$ are the MacCauley brackets, such that

$$\langle\circ\rangle = \frac{\circ + |\circ|}{2} \tag{5}$$

f_{P} is a rate-independent yield function, usually dependent on the equivalent plastic strain

$$f_{\mathrm{P}} = \bar{\sigma} - \sigma_{\mathrm{Y}}(\bar{\varepsilon}^{\mathrm{p}}) \tag{6}$$

κ is a viscosity parameter and Φ is the overstress function, commonly given by a potential law

$$\Phi(f_{\mathrm{P}}) = \left(\frac{f_{\mathrm{P}}}{\sigma_{\mathrm{Y}}(\bar{\varepsilon}^{\mathrm{p}})}\right)^{m} \tag{7}$$

m being a constant. The viscosity parameter κ and the constants in Φ are material-dependent so, they should be obtained from experimental results. From the explicit definition of the plastic multiplier given by Eq. (4) it is clear that plastic flow can take place only if $\Phi(f_{\mathrm{P}})$ is greater than zero, that is $f_{\mathrm{P}} > 0$, and stress may be above the yield surface leading to the overstress.

2.2. Wang consistency model

Rate-dependent plasticity can also be formulated by including the rate of the state variables in the yield function, leading to the consistency model first proposed by Wang (1997) and Wang et al. (1997). Following the notation proposed by Heeres et al. (2002), the rate-dependent yield surface is given by

$$f_{\mathrm{RD}} = f_{\mathrm{RD}}(\sigma, \vec{\kappa}, \dot{\vec{\kappa}}) \tag{8}$$

Assuming that the only state variable is the equivalent plastic strain $\vec{\kappa} = \bar{\varepsilon}^{\mathrm{p}}$, and J_2 plasticity $\dot{\bar{\varepsilon}}^{\mathrm{p}} = \dot{\lambda}$, derivation of the yield function leads to

$$\dot{f}_{\mathrm{RD}} = \frac{\partial f_{\mathrm{RD}}}{\partial \sigma} : \dot{\sigma} + \frac{\partial f_{\mathrm{RD}}}{\partial \lambda}\dot{\lambda} + \frac{\partial f_{\mathrm{RD}}}{\partial \dot{\lambda}}\ddot{\lambda} \tag{9}$$

In this model, the plastic multiplier and the stress are assumed to obey certain unilateral constraints: the Kuhn–Tucker loading/unloading complementary conditions, classical in the convex mathematical programming literature, are given by

$$\lambda \geqslant 0, \quad f_{\mathrm{RD}} \leqslant 0, \quad \lambda f_{\mathrm{RD}} = 0 \tag{10}$$

These conditions indicate that the stress must be admissible and that plastic flow can take place only on the yield surface given by Eq. (7). Additionally, the so-called consistency (or persistency) condition is proposed

$$\lambda \dot{f}_{\mathrm{RD}} = 0 \tag{11}$$

which corresponds to the requirement that the stress must persist on the yield surface for an increase of λ (Simo and Hughes, 1998). It is obvious that neither Kuhn–Tucker nor consistency conditions are applicable in the Perzyna model. On the contrary, in the Wang consistency model plastic flow arises when $f_{\mathrm{RD}} = 0$ (with no overstress), and the unloading process is always elastic ($f_{\mathrm{RD}} < 0$).

2.3. Comparison of the Perzyna overstress models and the Wang consistency model

Recently a systematic comparison of the above models by Heeres et al. (2002) has lead to the following conclusions:

- The plastic multiplier evolution is defined explicitly in the Perzyna model (Eq. (4)), while in the Wang consistency model it is defined by the second-order differential equation

$$\dot{f}_{\mathrm{RD}} = 0 \tag{12}$$

  $\dot{f}_{\mathrm{RD}}$ being defined by Eq. (9).
- During plastic loading, both models lead to identical results if the following conditions are fulfilled

$$\frac{\partial f_{\mathrm{P}}}{\partial \sigma} = \frac{\partial f_{\mathrm{RD}}}{\partial \sigma} \tag{13}$$

$$-\frac{\partial f_{\mathrm{RD}}}{\partial \dot{\lambda}} = \eta \left(\frac{\mathrm{d}\Phi}{\mathrm{d}f_{\mathrm{P}}}\right)^{-1} \tag{14}$$

- During unloading, the Perzyna model leads to plastic deformation so long as overstress is present, whereas the consistency model always unloads elastically. Consequently the evolution of the state variables is different during stress reversals.
- The Wang consistency model yields a somewhat higher convergence rate than that derived by the Perzyna model.

2.4. Consistency and thermoviscoplasticity

Plastic instabilities arising in high strain rate deformation are commonly triggered by an adiabatic increase of temperature, which strongly reduces the rate of strain-hardening of most metals and alloys (Rusinek and Klepaczko, 2001). Thus, for a proper simulation of manufacturing processes such as

high-speed metal forming and cutting, or the service life impulsive loading of structural elements (crash, ballistic impact), the effect of temperature should be considered as a key point of the description of the material behaviour. The main aims of this work were to include thermal effects in the Consistency viscoplasticity model and to develop robust algorithms to integrate it, keeping in mind that in these applications the spatial configuration of the solid diverges notably from the material one and a large deformation frame has to be considered.

3. Consistency thermoviscoplastic constitutive equations at finite deformations

3.1. Basic kinematics of finite deformations

Let $\mathbf{B}_0 \subset \mathbb{R}^3$ be the initial, reference or undeformed configuration of a body (considered coincident); the motion of the body is described by a function $\varphi:\mathbf{B}_0 \to \mathbf{B}_t \subset \mathbb{R}^3$ which maps a material point X into the spatial point $x = \varphi(X,t)$. The deformation gradient F is defined by

$$F = \nabla_0 x = \frac{\partial x}{\partial X} \tag{15}$$

This tensor transforms a material vector $\mathrm{d}X$ into the corresponding spatial vector $\mathrm{d}x$

$$\mathrm{d}x = F\mathrm{d}X \tag{16}$$

According to the polar decomposition theorem, F may be decomposed as

$$F = RU = VR \tag{17}$$

R being the polar orthogonal rotation tensor, U the material or right stretch tensor and V the spatial or left stretch tensor. The velocity of a particle v is defined as the time derivative of φ

$$v(X,t) = \frac{\partial \varphi(X,t)}{\partial t} \tag{18}$$

This spatial vector is defined more consistently as a function of the spatial position

$$v(x,t) = v(\varphi^{-1}(x,t),t) \tag{19}$$

Spatial derivative of this expression leads to the velocity gradient tensor l

$$l = \nabla_x v = \frac{\partial v(x,t)}{\partial x} \tag{20}$$

which is given by

$$l = \dot{F}F^{-1} \tag{21}$$

The velocity gradient tensor can be decomposed into symmetric and skew-symmetric parts by

$$d = \frac{1}{2}(l + l^{\mathrm{T}}) \tag{22}$$

$$w = \frac{1}{2}(l - l^{\mathrm{T}}) \tag{23}$$

where d is the rate of deformation tensor and w the spin tensor.

3.2. Additive decomposition of the rate of deformation tensor

For structural materials used in crashworthiness, machining or ballistic applications, elastic and thermal strains (and rates) are commonly very small compared to unity or to plastic strains (and rates). Taking advantage of this behaviour, the description of the deformation may be simplified. Starting from the multiplicative decomposition

$$F = F^{e} F^{\theta} F^{p} \tag{24}$$

we may write the spatial velocity gradient as

$$l = \dot{F} F^{-1} = l^{e} + F^{e} l^{\theta} F^{e^{-1}} + F^{e} \dot{F}^{\theta} l^{p} F^{\theta^{-1}} F^{e^{-1}} \tag{25}$$

l^{e}, l^{θ} and l^{p} being the elastic, thermal and plastic spatial velocity gradients defined as

$$l^{e} = \dot{F}^{e} F^{e^{-1}}, \quad l^{\theta} = \dot{F}^{\theta} F^{\theta^{-1}}, \quad l^{p} = \dot{F}^{p} F^{p^{-1}} \tag{26}$$

From the left polar decomposition of the deformation gradient (uncoupling rigid body from elastic, thermal and plastic deformation)

$$F = V^{e} V^{\theta} V^{p} R \tag{27}$$

where the different V are the left stretch tensors. Using the nominal strain tensor ϵ as a measure for small elastic and thermal deformations, we have

$$F^{e} = V^{e} = 1 + \epsilon^{e} \approx 1 \tag{28}$$

$$F^{\theta} = V^{\theta} = 1 + \epsilon^{\theta} \approx 1 \tag{29}$$

and Eq. (25) leads to the additive decomposition of the velocity gradient

$$l = \dot{F} F^{-1} \approx l^{e} + l^{\theta} + l^{p} \tag{30}$$

Taking the symmetric part of Eq. (30) we obtain the additive decomposition of the rate of deformation tensor d generally assumed for hypoelastic–plastic materials (Nemat-Nasser, 1982; Khan and Huang, 1995).

$$d \approx d^{e} + d^{\theta} + d^{p} \tag{31}$$

3.3. Constitutive equations

The elastic stress–strain relation is given by

$$\sigma^{\nabla} = C : \; d^{e} = C : (d - d^{\theta} - d^{p}) \tag{32}$$

σ^{∇} being an objective stress rate and C the linear isotropic elastic tensor defined by the fourth order tensorial equation

$$C = 2GI_{\mathrm{dev}} + K1 \otimes 1 \tag{33}$$

with G and K elastic constants

$$G = \frac{E}{2(1+v)} \tag{34}$$

$$K = \frac{E}{3(1-2v)} \tag{35}$$

I is the unit fourth order tensor exhibiting only minor symmetry

$$(I)_{ijkl} = \delta_{ik}\delta_{jl} \tag{36}$$

and I_{dev} the deviatoric projector

$$I_{\text{dev}} = I - \frac{1}{3} 1 \otimes 1 \tag{37}$$

1 being the unit second order tensor

$$(1)_{ij} = \delta_{ij} \tag{38}$$

Assuming Mises plasticity with isotropic hardening, the yield function f is written as

$$f = \bar{\sigma} - \sigma_{\text{Y}}(\bar{\varepsilon}^{\text{p}}, \dot{\bar{\varepsilon}}^{\text{p}}, \theta) \tag{39}$$

where θ is the temperature, $\bar{\sigma}$ is the equivalent stress, that could be expressed in terms of the deviatoric stress s as

$$\bar{\sigma} = \sqrt{\frac{3}{2} s : s} \tag{40}$$

$\dot{\bar{\varepsilon}}^{\text{p}}$ is the equivalent plastic strain rate given by

$$\dot{\bar{\varepsilon}}^{\text{p}} = \sqrt{\frac{2}{3} d^{\text{p}} : d^{\text{p}}} \tag{41}$$

and $\bar{\varepsilon}^{\text{p}}$ the accumulated or equivalent plastic strain, defined by

$$\bar{\varepsilon}^{\text{p}} = \int_0^t \dot{\bar{\varepsilon}}^{\text{p}}(\tau)\, \mathrm{d}\tau \tag{42}$$

The yield function defines the yield surface $f = 0$ and the elastic domain $f \leqslant 0$. Choosing an associative plastic flow rule, the plastic strain rate is given by

$$d^{\text{p}} = \dot{\lambda} f_{\sigma} = \dot{\lambda} r \tag{43}$$

where λ is the plastic multiplier and r the direction of the plastic flow given by the deviatoric tensor

$$r = \frac{3}{2} \frac{s}{\bar{\sigma}} \tag{44}$$

From Eqs. (40), (41) and (44) it could be stated that in J_2 plasticity

$$\dot{\bar{\varepsilon}}^{\text{p}} = \dot{\lambda} \tag{45}$$

and hence the equivalence of the plastic multiplier and the equivalent plastic strain

$$\bar{\varepsilon}^{\text{p}} = \lambda \tag{46}$$

The thermal strain rate for isotropic materials is written

$$d^{\theta} = \alpha \dot{\theta} 1 \tag{47}$$

where α is the coefficient of thermal expansion. If adiabatic behaviour is assumed (no heat flux takes place) and only plastic work is considered as the volumetric heat source, heating is determined by equation

$$\dot{\theta} = \eta \frac{\sigma : d^{\text{p}}}{\rho c_v} \tag{48}$$

ρ being the density, c_v the specific heat and η the Quinney–Taylor coefficient. The solution of Eqs. (32), (43), (45), (47) and (48) must be subjected to the Kuhn–Tucker complementary conditions

$$\lambda \geqslant 0, \quad f \leqslant 0, \quad \lambda f = 0 \tag{49}$$

and the consistency condition

$$\lambda \dot{f} = 0 \tag{50}$$

4. Integration scheme and solving algorithm

To integrate the above rate equations, incremental objectivity is achieved by rewriting them in a neutralized configuration (Simo and Hughes, 1998; Doghri, 2000; Hagege, 2004). To formalize this approach, being ϖ a spatial skew-symmetric tensor, we may generate a group of rotations $\mathfrak{R}$ such that

$$\dot{\mathfrak{R}} = \varpi \mathfrak{R}, \quad \mathfrak{R}_{(t=0)} = I \tag{51}$$

with

$$\varpi = -\varpi^{\mathrm{T}} \tag{52}$$

and

$$\mathfrak{R}^{-1} = \mathfrak{R}^{\mathrm{T}} \tag{53}$$

Typical choices of ϖ include the spin tensor w and the tensor Ω defined as

$$\Omega = \dot{R} R^{\mathrm{T}} \tag{54}$$

where R is the polar rotation tensor. The Cauchy stress tensor and the rate of deformation tensor are rotated as

$$\sigma_{\mathfrak{R}} = \mathfrak{R}^{\mathrm{T}} \sigma \mathfrak{R}, \quad d_{\mathfrak{R}} = \mathfrak{R}^{\mathrm{T}} d \mathfrak{R} \tag{55}$$

Observe that time differentiation of the rotated Cauchy stress leads to

$$\dot{\sigma}_{\mathfrak{R}} = \mathfrak{R}^{\mathrm{T}} (\dot{\sigma} + \sigma\varpi - \varpi\sigma) \mathfrak{R} = \mathfrak{R}^{\mathrm{T}} \sigma^{\nabla} \mathfrak{R} \tag{56}$$

σ^{∇}coincides with the Green–Naghdi–McInnis stress rate if $\varpi = \Omega$ (and then $\mathfrak{R} = R$) or with the Jaumann stress rate if $\varpi = w$ (see Simo and Hughes (1998) for a description of the algorithm to integrate Eq. (51) in this case). Thus, a complicated objective stress rate can be computed as a simple time derivative. Moreover, taking advantage of the orthogonality of $\mathfrak{R}$, the symmetry of the Cauchy stress and rate of deformation tensors and the isotropy of the elastic tensor ($C_{\mathfrak{R}} = C$), the rate equations defined above are form-identical in the rotated configuration

$$\dot{\sigma}_{\mathfrak{R}} = C : \; d^{\mathrm{e}}_{\mathfrak{R}} = C : (d_{\mathfrak{R}} - d^{\theta}_{\mathfrak{R}} - d^{\mathrm{p}}_{\mathfrak{R}}) \tag{57}$$

$$\bar{\sigma} = \sqrt{\frac{3}{2} s_{\mathfrak{R}} : s_{\mathfrak{R}}}, \quad \dot{\bar{\varepsilon}}^{\mathrm{p}} = \sqrt{\frac{2}{3} d^{\mathrm{p}}_{\mathfrak{R}} : d^{\mathrm{p}}_{\mathfrak{R}}}, \quad \dot{\theta} = \eta \frac{\sigma_{\mathfrak{R}} : d^{\mathrm{p}}_{\mathfrak{R}}}{\rho c_v} \tag{58}$$

$$f \equiv \bar{\sigma} - \sigma_{\mathrm{Y}}(\bar{\varepsilon}^{\mathrm{p}}, \dot{\bar{\varepsilon}}^{\mathrm{p}}, \theta) = 0 \tag{59}$$

$$d^{\mathrm{p}}_{\mathfrak{R}} = \dot{\lambda} r_{\mathfrak{R}} = \dot{\lambda} \frac{3}{2} \frac{s_{\mathfrak{R}}}{\bar{\sigma}} \tag{60}$$

$$d^{\theta}_{\mathfrak{R}} = \alpha \dot{\theta} I \tag{61}$$

4.1. The solving algorithm

Within the neutralized configuration, the classical return mapping algorithm is proposed to solve the preceding equations (Simo and Hughes, 1998; Doghri, 2000). Return is performed at time $n+1$ with the corresponding updated rotated stress

$$\sigma_{\Re_{n+1}} = \sigma^{\text{trial}}_{\Re_{n+1}} + \Delta\sigma^{\theta}_{\Re} + \Delta\sigma^{\text{ret}}_{\Re} \tag{62}$$

where rotated trial stress is given by

$$\sigma^{\text{trial}}_{\Re_{n+1}} = \sigma_{\Re_n} + C : (\Delta\varepsilon_{\Re}) \tag{63}$$

$\sigma_{\Re_n}$ being the rotated stress at time n

$$\sigma_{\Re_n} = \Re^{\mathrm{T}}_n \sigma_n \Re_n \tag{64}$$

and $\Delta\varepsilon_{\Re}$ the increment of total deformation in the neutralized frame, which could be obtained by an objective approximation of the rate of deformation tensor $d_{n+1/2}$ calculated by the midpoint rule (see Simo and Hughes, 1998; Doghri, 2000)

$$\Delta\varepsilon_{\Re} = \Delta t d_{\Re_{n+1/2}} = \Delta t \Re^{\mathrm{T}}_{n+1/2} d_{n+1/2} \Re_{n+1/2} \tag{65}$$

A fully implicit Backward–Euler scheme is used to obtain corrections to the trial stress

$$\Delta\sigma^{\text{ret}}_{\Re} = -C : \left(\frac{3}{2}\Delta\lambda \frac{s_{\Re_{n+1}}}{\bar{\sigma}_{n+1}}\right) = -3G\Delta\lambda \frac{s_{\Re_{n+1}}}{\bar{\sigma}_{n+1}} \tag{66}$$

$$\Delta\sigma^{\theta}_{\Re} = -C : (\alpha\Delta\theta I) = -3K\alpha\Delta\theta I \tag{67}$$

The updated deviatoric stress is given by

$$s_{\Re_{n+1}} = I_{\text{dev}} : (\sigma^{\text{trial}}_{\Re_{n+1}} + \Delta\sigma^{\theta}_{\Re} + \Delta\sigma^{\text{ret}}_{\Re}) = s^{\text{trial}}_{\Re_{n+1}} - 3G\Delta\lambda \frac{s_{\Re_{n+1}}}{\bar{\sigma}_{n+1}} \tag{68}$$

This last equation clearly shows the proportionality between $s_{\Re_{n+1}}$ and $s^{\text{trial}}_{\Re_{n+1}}$, which could equally be stated as

$$\frac{s_{\Re_{n+1}}}{\bar{\sigma}_{n+1}} = \frac{s^{\text{trial}}_{\Re_{n+1}}}{\bar{\sigma}^{\text{trial}}_{n+1}} \tag{69}$$

According to the Backward–Euler method being used, an implicit rule is selected to approximate the temperature increase, yielding the following expression

$$\Delta\theta = \frac{3}{2}\frac{\eta\Delta\lambda}{\rho_{n+1}c_v\bar{\sigma}_{n+1}}\sigma_{\Re_{n+1}} : s_{\Re_{n+1}} = \frac{3}{2}\frac{\eta\Delta\lambda}{\rho_{n+1}c_v\bar{\sigma}_{n+1}}(\sigma^{\text{trial}}_{\Re_{n+1}} + \Delta\sigma^{\text{ret}}_{\Re} + \Delta\sigma^{\theta}_{\Re}) :$$
$$s_{\Re_{n+1}} = \frac{\eta}{\rho_{n+1}c_v}(\bar{\sigma}^{\text{trial}}_{n+1}\Delta\lambda - 3G\Delta\lambda^2) = \frac{\eta}{\rho_{n+1}c_v}\bar{\sigma}_{n+1}\Delta\lambda \tag{70}$$

Updated density is given by

$$\rho_{n+1} = \frac{\rho_0}{\det(F)} \tag{71}$$

From Eqs. (27)–(29), $\det(F)$ is approximated by

$$\det(F) = \det(F^{\mathrm{e}})\det(F^{\theta}) \approx \det(I + \epsilon^{\mathrm{e}})\det(I + \epsilon^{\theta}) \approx 1 + \operatorname{tr}(\epsilon^{\mathrm{e}}) + \operatorname{tr}(\epsilon^{\theta}) = 1 + \operatorname{tr}(\epsilon) \tag{72}$$

and ρ_{n+1} could be written in terms of the trace of a total strain measurement, i.e. the cumulative corrotational strain

$$\rho_{n+1} \approx \frac{\rho_0}{(1 + I : \varepsilon_{\Re_{n+1}})} \tag{73}$$

Thus the terms in Eq. (62) are known once the increment of the plastic multiplier $\Delta\lambda$ is obtained by imposing the consistency condition. According to the *consistency model*, in a plastic increment the yield condition for the equivalent stress, effective plastic strain, effective plastic strain rate and temperature has to be satisfied at time t_{n+1}, thus avoiding overstress. As stated previously, in J_2 plasticity $\dot{\bar{\varepsilon}}^{\mathrm{p}} = \dot{\lambda}$, and the consistency condition could be formulated as

$$f_{n+1} = f(\bar{\sigma}_{n+1}, \lambda_{n+1}, \dot{\lambda}_{n+1}, \theta_{n+1}) = 0 \tag{74}$$

In their consistency model Winnicki et al. (2001) proposed an approximation for $\dot{\lambda}$ as

$$\dot{\lambda} = \frac{\Delta\lambda}{\Delta t} \tag{75}$$

On this assumption, the consistency condition is then rewritten in terms of the initial values and the plastic multiplier increment leading to a non-linear algebraic equation in the variable $\Delta\lambda$.

$$f\left(\bar{\sigma}_{n+1}^{\mathrm{trial}} - 3G\Delta\lambda, \lambda_n + \Delta\lambda, \frac{\Delta\lambda}{\Delta t}, \theta_n + \frac{\eta}{\rho_{n+1} c_v}(\bar{\sigma}_{n+1}^{\mathrm{trial}}\Delta\lambda - 3G\Delta\lambda^2)\right) = 0 \tag{76}$$

If an iterative Newton–Raphson procedure is used to find the root $\Delta\lambda$, linearization of this equation leads to

$$f^{(k+1)} \approx f^{(k)} - 3G\delta\lambda^{(k)} - H^{(k)}\delta\lambda^{(k)} - S^{(k)}\frac{\delta\lambda^{(k)}}{\Delta t} - T^{(k)}\frac{\eta}{\rho_{n+1} c_v}(\bar{\sigma}_{n+1}^{\mathrm{trial}}\delta\lambda^{(k)} - 6G\Delta\lambda^{(k)}\delta\lambda^{(k)}) = 0 \tag{77}$$

In the last expressions, k is the iteration index, H is the plastic modulus, S the viscoplastic modulus and T the temperature sensitivity

$$H = -f_{\bar{\varepsilon}^{\mathrm{p}}} = -f_{\lambda} \tag{78}$$

$$S = -f_{\dot{\bar{\varepsilon}}^{\mathrm{p}}} = -f_{\dot{\lambda}} \tag{79}$$

$$T = -f_{\theta} \tag{80}$$

From this equation, $\delta\lambda^{(k)}$ could be calculated as:

$$\delta\lambda^{(k)} = \frac{f^{(k)}}{3G + H^{(k)} + \frac{S^{(k)}}{\Delta t} + T^{(k)}\frac{\eta}{\rho_{n+1} c_v}(\bar{\sigma}_{n+1}^{\mathrm{trial}} - 6G\Delta\lambda^{(k)})} \tag{81}$$

It is obvious that the classical radial return algorithm (Wilkins, 1964) for strain hardening Mises plasticity is recovered if no strain rate and temperature effects are considered ($S = T = 0$). Note that the viscosity parameter used (see Ponthot, 2002) to obtain $\delta\lambda$ for overstress models is here substituted by the strain-rate sensitivity S derived directly from the hardening relation, as a result of including rate effects in the yield function (consistency). Also thermal softening is directly coupled to the return mapping algorithm since temperature was considered as an element of the hardening relation.

$\Delta\lambda$ is updated after every iteration

$$\Delta\lambda^{(k+1)} = \Delta\lambda^{(k)} + \delta\lambda^{(k)} \tag{82}$$

and the Newton–Raphson scheme is used until $f^{(k+1)}$ is lower than the tolerance. All the variables could then be determined from the final value of $\Delta\lambda$. To increase the efficiency of the algorithm, the final value

of $\Delta\lambda$ could be stored and used as the initial value in the Newton–Raphson iteration process for the next time increment at the same integration point, if plastic flow takes place.

We considered constant values for the Quinney–Taylor coefficient η. However, recent works have shown that this coefficient is not a constant but a function of plastic strain and plastic strain rate (see Hodowany et al., 2000). The algorithm developed suggests its dependence on $\bar{\varepsilon}^{\mathrm{p}}$ and $\dot{\bar{\varepsilon}}^{\mathrm{p}}$ in an implicit way since both arguments are state variables. Linearization of the consistency equation should take into account this dependence. Then, Eq. (81) becomes

$$\delta\lambda^{(k)} = f^{(k)}\left[3G + H^{(k)} + \frac{S^{(k)}}{\Delta t} + \frac{T^{(k)}}{\rho_{n+1}c_v}(\eta^{(k)}(\bar{\sigma}^{\mathrm{trial}}_{n+1} - 6G\Delta\lambda^{(k)}) + (\Lambda^{(k)} + \Gamma^{(k)}\Delta t^{-1})(\bar{\sigma}^{\mathrm{trial}}_{n+1}\Delta\lambda^{(k)} - 3G\Delta\lambda^{(k)^2}))\right]^{-1} \tag{83}$$

where

$$\Lambda = \eta_{\bar{\varepsilon}^{\mathrm{p}}} \tag{84}$$

and

$$\Gamma = \eta_{\dot{\bar{\varepsilon}}^{\mathrm{p}}} \tag{85}$$

Once $\Delta\lambda$ has been obtained, the updated rotated stress is pushed to the spatial configuration by $\mathfrak{R}_{n+1}$, leading to the following expression

$$\sigma_{n+1} = \Delta\mathfrak{R}^{n+1}_n \sigma_n \Delta\mathfrak{R}^{n+1^{\mathrm{T}}}_n + C : (\Delta\mathfrak{R}^{n+1}_{n+1/2} d_{n+1/2} \Delta\mathfrak{R}^{n+1^{\mathrm{T}}}_{n+1/2}) - \frac{3G\Delta\lambda}{\bar{\sigma}^{\mathrm{trial}}_{n+1}} \mathfrak{R}_{n+1} s^{\mathrm{trial}}_{\mathfrak{R}_{n+1}} \mathfrak{R}^{\mathrm{T}}_{n+1} - \frac{3K\alpha\eta}{\rho_{n+1}c_v}\bar{\sigma}_{n+1}\Delta\lambda I \tag{86}$$

where the incremental rotation tensors are given by

$$\Delta\mathfrak{R}^{n+1}_n = \mathfrak{R}_{n+1}\mathfrak{R}^{\mathrm{T}}_n \tag{87}$$

$$\Delta\mathfrak{R}^{n+1}_{n+1/2} = \mathfrak{R}_{n+1}\mathfrak{R}^{\mathrm{T}}_{n+1/2} \tag{88}$$

4.2. Consistent tangent operator

When a Newton method is used to approximate to the weak form of equilibrium, a global Jacobian matrix is computed by assembling local tangent operators. The asymptotic rate of quadratic convergence is achieved by using the consistent tangent operator $\mathbb{T}^{\mathrm{alg}}$ instead of the continuum one (Simo et al., 1985). $\mathbb{T}^{\mathrm{alg}}$ could be obtained for the proposed algorithm by the procedure described in Doghri (2000): first the rotated consistent tangent operator $\mathbb{T}^{\mathrm{alg}}_{\mathfrak{R}}$ is found from the infinitesimal scheme in the neutralized frame and then it is rotated with $\mathfrak{R}_{n+1}$. A similar algorithmic strategy was used by Nagtegaal (1982) and Lin and Brocks (2004).

The rotated operator is determined by letting variables vary slightly about the converged solution. A differentiation of elastic stress–strain relation, discretized temperature increase, discretized plastic flow rule and yield condition gives the following equations, where the Quinney–Taylor coefficient is considered constant and subscript $(n+1)$ is omitted for simplicity

$$\delta\sigma_{\mathfrak{R}} = C : \delta\varepsilon_{\mathfrak{R}} - C : \delta\varepsilon^{\theta}_{\mathfrak{R}} - C : \delta\varepsilon^{p}_{\mathfrak{R}} \tag{89}$$

$$C : \delta\varepsilon^{\theta}_{\mathfrak{R}} = \frac{3K\alpha\eta}{c_v}\left(\frac{I : \delta\varepsilon_{\mathfrak{R}}}{\rho_0}\bar{\sigma}\Delta\lambda + \frac{1}{\rho}r_{\mathfrak{R}} : \delta\sigma_{\mathfrak{R}}\Delta\lambda + \frac{1}{\rho}\bar{\sigma}\delta\lambda\right)I \tag{90}$$

$$C: \ \delta\varepsilon^p_{\Re} = 2Gr_{\Re}\delta\lambda + 2G\frac{\partial r_{\Re}}{\partial\sigma_{\Re}} : \delta\sigma_{\Re}\Delta\lambda \tag{91}$$

$$r_{\Re} : \delta\sigma_{\Re} - H\delta\lambda - S\frac{\delta\lambda}{\Delta t} - T\frac{\eta}{c_v}\left(\frac{I : \delta\varepsilon_{\Re}}{\rho_0}\bar{\sigma}\Delta\lambda + \frac{1}{\rho}r_{\Re} : \delta\sigma_{\Re}\Delta\lambda + \frac{1}{\rho}\bar{\sigma}\delta\lambda\right) = 0 \tag{92}$$

Substituting Eqs. (90) and (91) in (89) and this last in the consistency condition (92), $\delta\lambda$ is deduced

$$\delta\lambda = \frac{1}{h}\left[r_{\Re} : C : \ \left(\delta\varepsilon_{\Re} - \frac{\partial r_{\Re}}{\partial\sigma_{\Re}} : \delta\sigma_{\Re}\Delta\lambda\right) - T\frac{\eta}{c_v}\left(\frac{I : \delta\varepsilon_{\Re}}{\rho_0}\bar{\sigma}\Delta\lambda + \frac{1}{\rho}r_{\Re} : \delta\sigma_{\Re}\Delta\lambda\right)\right] \tag{93}$$

in which

$$h = 3G + H + \frac{S}{\Delta t} + T\frac{\eta}{\rho c_v}\bar{\sigma} \tag{94}$$

With this value of $\delta\lambda$, Eqs. (90) and (91) are again substituted in (89) and, accounting for the condition

$$r_{\Re} : C : \ \frac{\partial r_{\Re}}{\partial\sigma_{\Re}} = 0 \tag{95}$$

the following relation between $\delta\sigma_{\Re}$ and $\delta\varepsilon_{\Re}$ is derived after a straightforward calculation

$$\mathbb{M}_{\Re} : \delta\sigma_{\Re} = \mathbb{H}_{\Re} : \delta\varepsilon_{\Re} \tag{96}$$

$\mathbb{M}_{\Re}$ and $\mathbb{H}_{\Re}$ being given by the following formulae

$$\mathbb{M}_{\Re} = I + 2G\Delta\lambda\frac{\partial r_{\Re}}{\partial\sigma_{\Re}} - 2GT\frac{\eta}{\rho c_v}\frac{\Delta\lambda}{h}r_{\Re}\otimes r_{\Re} + 3K\frac{\alpha\eta}{\rho c_v}\Delta\lambda\left(1 - T\frac{\eta}{\rho c_v}\frac{\bar{\sigma}}{h}\right)1\otimes r_{\Re} \tag{97}$$

$$\mathbb{H}_{\Re} = C - \frac{4G^2}{h}r_{\Re}\otimes r_{\Re} - 3K\frac{\alpha\eta}{\rho_0 c_v}\bar{\sigma}\Delta\lambda\left(1 - T\frac{\eta}{\rho c_v}\frac{\bar{\sigma}}{h}\right)1\otimes 1 - 6KG\frac{\alpha\eta}{\rho c_v}\frac{\bar{\sigma}}{h}1\otimes r_{\Re} + 2GT\frac{\eta}{\rho_0 c_v}\frac{\bar{\sigma}\Delta\lambda}{h}r_{\Re}\otimes 1 \tag{98}$$

the Hessian of J_2 yield function being given by

$$\frac{\partial r_{\Re}}{\partial\sigma_{\Re}} = \frac{1}{\bar{\sigma}}\left(\frac{3}{2}\left(I - \frac{1}{3}1\otimes 1\right) - r_{\Re}\otimes r_{\Re}\right) \tag{99}$$

After inverting $\mathbb{M}_{\Re}$

$$\mathbb{M}^{-1}_{\Re} = \frac{\bar{\sigma}}{3G\Delta\lambda + \bar{\sigma}}I + 2G\Delta\lambda\left(\frac{1}{3G\Delta\lambda + \bar{\sigma}} + \frac{T\eta}{h\rho c_v - 3GT\Delta\lambda\eta}\right)r_{\Re}\otimes r_{\Re} + \frac{3K\alpha\Delta\lambda\eta(T\eta\bar{\sigma} - h\rho c_v)}{\rho c_v(h\rho c_v - 3GT\Delta\lambda\eta)}1\otimes r_{\Re} + \frac{G\Delta\lambda}{3G\Delta\lambda + \bar{\sigma}}1\otimes 1 \tag{100}$$

the rotated consistent tangent operator is given by

$$\mathbb{T}^{\mathrm{alg}}_{\Re} = \mathbb{M}^{-1}_{\Re} : \mathbb{H}_{\Re} = T_1 I + T_2 r_{\Re}\otimes r_{\Re} + T_3 r_{\Re}\otimes 1 + T_4 1\otimes r_{\Re} + T_5 1\otimes 1 \tag{101}$$

with

$$T_1 = \frac{2G\bar{\sigma}}{3G\Delta\lambda + \bar{\sigma}} \tag{102}$$

$$T_2 = \frac{4G^2(-T\Delta\lambda\eta\bar{\sigma} + \rho c_v(3G\Delta\lambda - h\Delta\lambda + \bar{\sigma}))}{(3G\Delta\lambda + \bar{\sigma})(3GT\Delta\lambda\eta - h\rho c_v)} \tag{103}$$

$$T_3 = \frac{2GT\Delta\lambda\eta\rho\bar{\sigma}}{\rho_0(-3GT\Delta\lambda\eta + h\rho c_v)} \tag{104}$$

$$T_4 = -\frac{6GK\alpha\eta(T\Delta\lambda\eta\bar{\sigma} - \rho c_v(\Delta\lambda(-3G + h) + \bar{\sigma}))}{\rho c_v(3GT\Delta\lambda\eta - h\rho c_v)} \tag{105}$$

$$T_5 = K - \frac{2G\bar{\sigma}}{3(3G\Delta\lambda + \bar{\sigma})} + \frac{3K\alpha\Delta\lambda\eta\bar{\sigma}(-T\eta\bar{\sigma} + h\rho c_v)}{\rho_0 c_v(3GT\Delta\lambda\eta - h\rho c_v)} \tag{106}$$

It should be noted that if $\Delta\lambda = 0$, $\mathbb{T}^{\mathrm{alg}}_{\mathfrak{R}}$ becomes a continuum relation between stress and strain rate accounting for thermal effects

$$\dot{\sigma}_{\mathfrak{R}} = \left(C - \frac{4G^2}{h} r_{\mathfrak{R}} \otimes r_{\mathfrak{R}} - 6KG\frac{\alpha\eta}{\rho c_v}\frac{\bar{\sigma}}{h} 1 \otimes r_{\mathfrak{R}}\right) : \dot{\varepsilon}_{\mathfrak{R}} \tag{107}$$

which leads to the classical continuum tangent operator for J_2 plasticity if no heating is considered.

Once $\mathbb{T}^{\mathrm{alg}}_{\mathfrak{R}}$ is obtained it is then pushed forward by $\mathfrak{R}_{n+1}$ to give $\mathbb{T}^{\mathrm{alg}}$

$$(\mathbb{T}^{\mathrm{alg}})_{ijkl} = (\mathfrak{R}_{n+1})_{iI}(\mathfrak{R}_{n+1})_{jJ}(\mathfrak{R}_{n+1})_{kK}(\mathfrak{R}_{n+1})_{lL}(\mathbb{T}^{\mathrm{alg}}_{\mathfrak{R}})_{IJKL} \tag{108}$$

5. Taylor impact test

The performance of the proposed algorithm is presented through a numerical example. Four Taylor impact tests were simulated with the Finite Element commercial code ABAQUS/Explicit (2003) in which the algorithm was implemented considering the Green–Naghdi–MacInnis stress rate. This test involves launching a circular cylinder at predetermined velocities against a hardened rigid target. The impacted end sustains a large amount of plastic deformation whose shape has been used over the years to estimate dynamic material properties by inverse numerical or analytical methods (Rule, 1997).

The Johnson–Cook hardening relation (Johnson and Cook, 1983) was selected for the simulation, although the proposed scheme is valid for any hardening rule of the form $\sigma_{\mathrm{Y}}(\bar{\varepsilon}^{\mathrm{p}}, \dot{\bar{\varepsilon}}^{\mathrm{p}}, \theta)$. There are more sophisticated hardening relations but the one due to Johnson and Cook is probably the most widely used among those accounting for plastic strain, plastic strain rate and temperature effects. Since numerous efforts have been made in the past to determine their properties for a large number of metallic materials, it has been implemented in many FE explicit codes. The relation is stated through the following multiplicative equation

$$\sigma_{\mathrm{Y}} = (A + B(\bar{\varepsilon}^{\mathrm{p}})^n)\left(1 + C\log\left(\frac{\dot{\bar{\varepsilon}}^{\mathrm{p}}}{\dot{\bar{\varepsilon}}_0}\right)\right)(1 - \Theta^m) \tag{109}$$

where Θ is the homologous temperature

$$\Theta = \frac{\theta - \theta_0}{\theta_m - \theta_0} \tag{110}$$

θ_0 being the reference temperature and θ_m the melting temperature. Concerning the plastic strain rate factor, it has to be considered that for $\dot{\bar{\varepsilon}}^{\mathrm{p}} < \dot{\bar{\varepsilon}}_0$ no strain rate sensitivity need be taken into account. Actually, the Johnson–Cook relation should be more properly defined as

$$\sigma_Y = (A + B(\bar{\varepsilon}^p)^n)\left(1 + C\log\left(\frac{\dot{\bar{\varepsilon}}^p}{\dot{\bar{\varepsilon}}_0}\right)\right)(1 - \Theta^m) \tag{111}$$

for $\dot{\bar{\varepsilon}}^p \geqslant \dot{\bar{\varepsilon}}_0$ and

$$\sigma_Y = (A + B(\bar{\varepsilon}^p)^n)(1 - \Theta^m) \tag{112}$$

for $\dot{\bar{\varepsilon}}^p < \dot{\bar{\varepsilon}}_0$. This leads to a discontinuity in the hardening relation, as well as in their derivatives H, S and T and the yield function $f(\Delta\lambda)$ itself, that has to be considered before starting the Newton–Raphson iteration process to guarantee convergence. If $f(\dot{\bar{\varepsilon}}_0\Delta t) > 0$, Eq. (111) should be used and $\Delta\lambda^{(0)} = \dot{\bar{\varepsilon}}_0\Delta t$ is then the seed value; otherwise, the solution starts from Eq. (112) and $\Delta\lambda^{(0)} = 0$ (Fig. 1).

The experimental data for this study were obtained from House (1989) Taylor test results for oxygen-free electronic copper (see Table 1 for properties). The initial length and diameter of the cylinders were respectively 56.96 mm and 7.595 mm, and specimens were launched at four different velocities: 153, 156, 180 and 189 m/s. Two measurements were considered for each deformed Taylor specimen, final length and mushroom diameter, and they were compared with the corresponding ones obtained with finite element simulations. These were performed using 0.3 mm characteristic size 8-node trilinear brick elements with reduced integration (*C3D8R* in ABAQUS notation) including hourglass control. Adaptative remeshing was

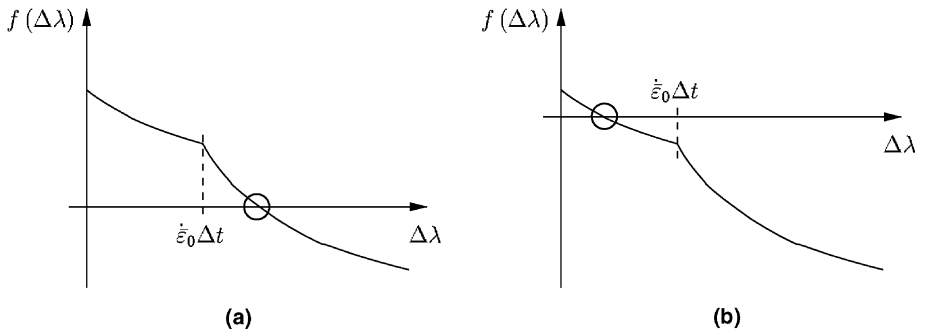

Fig. 1. Root after discontinuity (a) and root before discontinuity (b).

Table 1
Properties of OFHC copper. Johnson–Cook parameters from (Meyers, 1994)

Property	Value
E (GPa)	124
v	0.34
ρ_0 (kg/m^3)	8960
A (MPa)	90
B (MPa)	292
n	0.31
C	0.025
$\dot{\bar{\varepsilon}}_0$ (s^{-1})	1
m	1.09
θ_0 (K)	298
θ_m (K)	1331
η	0.9
c_v (m^2/s^2/K)	383
α (K^{-1})	1.7×10^{-5}

performed at each fifth time-increment to reduce mesh distortion and computational time. No friction was considered between projectile tip and rigid surface.

Plots of the calculated specimen dimensions versus measured Taylor specimen dimensions are shown in Figs. 2 and 3. Simulations slightly underestimate the final lengths and overestimate the mushroom diameter to some extent. The numerical results obtained with the Johnson–Cook model offered in the ABAQUS/Explicit material library are similar to those obtained with the user subroutine, with differences lower than 1%. Since the Johnson–Cook model assumes that the shapes of the strain-hardening curves are proportional to the quasi-static one through the multiplicative term $(1 + C\log(\dot{\bar{\varepsilon}}^{\mathrm{p}}/\dot{\bar{\varepsilon}}_0))$ (Eq. (109)), the plastic multiplier could be explicitly given by

$$\dot{\lambda} = \dot{\bar{\varepsilon}}^{\mathrm{p}} = \dot{\bar{\varepsilon}}_0 \exp\left(\frac{1}{C}\frac{\bar{\sigma} - \sigma_{\mathrm{Y}}(\bar{\varepsilon}^{\mathrm{p}}, \theta)}{\sigma_{\mathrm{Y}}(\bar{\varepsilon}^{\mathrm{p}}, \theta)}\right) \tag{113}$$

as in the overstress formulation. Nevertheless, the influence of strain rate on the yield stress is often more complex, and advanced hardening equations should be used, such as that proposed by Rusinek and Klepaczko (2001), which leads to no explicit expression of strain rate in terms of equivalent stress and state variables. In such cases the consistency model presents a good alternative to the overstress models.

The developed algorithm also allows a saving of values of strain rate at element integration points. In plotting strain rate contours, the evolution of the plastic wave is easily followed. Fig. 4 shows a longitudinal section of a Taylor cylinder where points with $\dot{\bar{\varepsilon}}^{\mathrm{p}} > 0$ are plotted at different instants of the impact process.

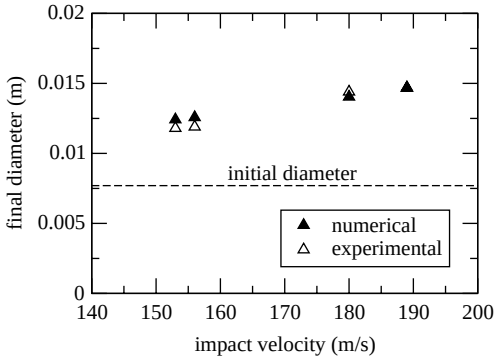

Fig. 2. Plot of calculated and measured projectile tip (mushroom) diameters versus velocity.

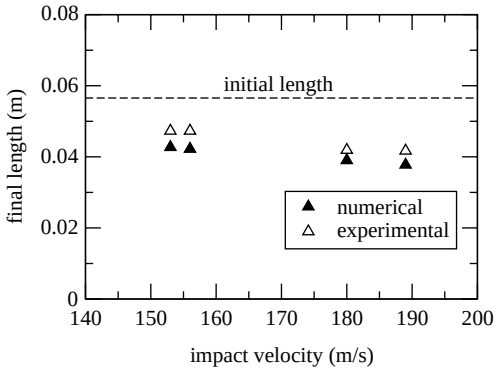

Fig. 3. Plot of calculated and measured final projectile lengths versus velocity.

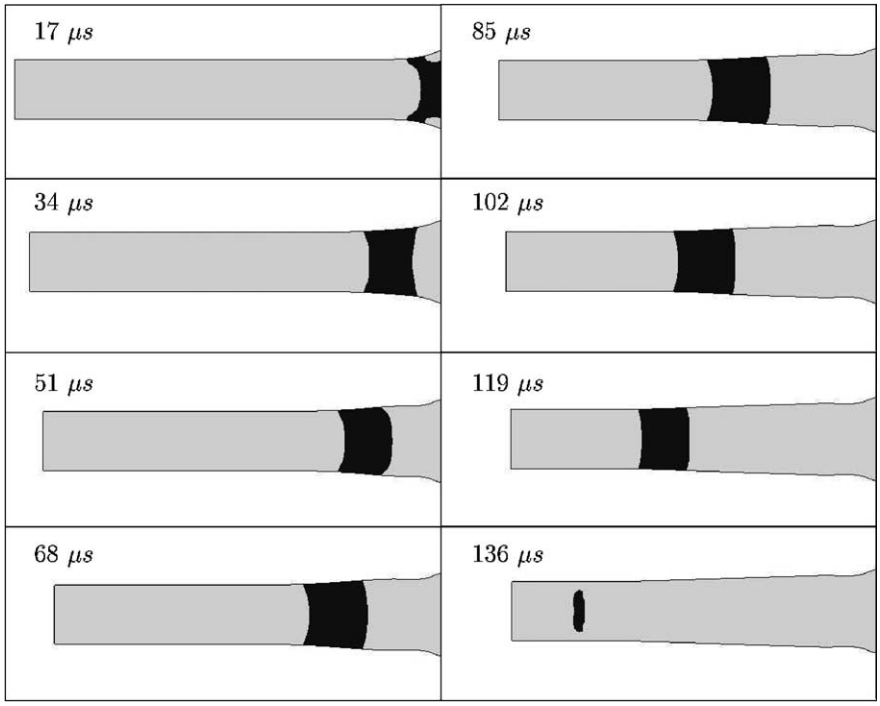

Fig. 4. Plastic wave position (points with $\dot{\bar{\varepsilon}}^{p} > 0$) during impact. Taylor test at 153 m/s.

It shows how the plastic wave is trapped at the projectile nose during the first stage of the process and leads to a localization of deformation in this zone. During the first microseconds, the plastic wave is slowed due to the reduced slope of plastic modulus H at high stress levels. As the stress level decreases, the plastic modulus increases and the inelastic wave accelerates to the rear end of the projectile. This gives rise to the conical shape characteristic of the deformed Taylor specimen.

6. Conclusions

A complete thermoviscoplastic fully implicit algorithm was derived and implemented in a finite element code. This allows a simulation of finite deformation processes in adiabatic conditions for any J_2 isotropic hardening yield function dependent on plastic strain, plastic strain rate and temperature.

Since a *consistency* viscoplasticity model was used, the algorithm enforces the equality of equivalent stress and yield stress for updated values of the state variables. Following the elastic predictor and plastic corrector scheme, it provides an expression of every updated variable in terms of the plastic multiplier increment, obtained by solving one non-linear scalar equation. The viscosity parameter, inherent in overstress models, is replaced by a viscoplastic modulus derived directly from the hardening relation of the material. Also, thermal softening effect is included in the return process. Moreover, a closed form of the consistent tangent operator was found.

The algorithm is easily implemented and inherits the robustness and stability of return mapping algorithms. The performance of the proposed algorithm is presented through several numerical simulations of the Taylor impact test. Their results agree quantitatively with the experimental results.

Acknowledgements

This research was done with the financial support of the Comunidad Autónoma de Madrid under Project 07N/0040/2002.

We wish to express sincere gratitude to Dr. B. Hagege for his valuable suggestions and his help with finite deformation formulation in ABAQUS/Explicit code, and to Dr. G. Asensio and Dr. J. Faleskog for helpful discussions.

Appendix. Overall algorithmic details for the corotational configuration

1. Elastic predictor

$$\sigma^{\text{trial}}_{\Re_{n+1}} = \sigma_{\Re_n} + C : (\Delta\varepsilon_{\Re}) \tag{114}$$

2. Check the yield condition

2.1. If $f(\bar{\sigma}^{\text{trial}}_{n+1}, \lambda_n, 0, \theta_n) \leqslant 0$

$$\sigma_{\Re_{n+1}} = \sigma^{\text{trial}}_{\Re_{n+1}}$$

$$\lambda_{n+1} = \lambda_n$$

$$\dot{\lambda}_{n+1} = 0$$

$$\theta_{n+1} = \theta_n$$

2.2. If $f(\bar{\sigma}^{\text{trial}}_{n+1}, \lambda_n, 0, \theta_n) > 0$

2.2.1. Initialization

$$\bar{\sigma}^{(0)}_{n+1} = \bar{\sigma}^{\text{trial}}_{n+1}$$

$$\Delta\lambda^{(0)} = 0$$

$$\lambda^{(0)}_{n+1} = \lambda_n$$

$$\dot{\lambda}^{(0)}_{n+1} = 0$$

$$\theta^{(0)}_{n+1} = \theta_n$$

2.2.2. Check convergence at kth iteration

$$f^{(k)} = f(\bar{\sigma}^{(k)}_{n+1}, \lambda^{(k)}_{n+1}, \dot{\lambda}^{(k)}_{n+1}, \theta^{(k)}_{n+1})$$

If $f^{(k)} <$ Tolerance $\Rightarrow$ Converged.

2.2.3. Compute increment $\delta\Delta\lambda^{(k)}$ with Eq. (81) using $\bar{\sigma}^{(k)}_{n+1}$, $\lambda^{(k)}_{n+1}$, $\dot{\lambda}^{(k)}_{n+1}$, $\theta^{(k)}_{n+1}$

2.2.4. Update state variables and equivalent stress

$$\Delta\lambda^{(k+1)} = \Delta\lambda^{(k)} + \delta\Delta\lambda^{(k)}$$

$$\lambda^{(k+1)}_{n+1} = \lambda^{(0)}_{n+1} + \Delta\lambda^{(k+1)}$$

$$\dot{\lambda}^{(k+1)}_{n+1} = \frac{\Delta\lambda^{(k+1)}}{\Delta t}$$

$$\theta_{n+1}^{(k+1)} = \theta_{n+1}^{(0)} + \eta \frac{(\Delta\lambda^{(k+1)}\bar{\sigma}_{n+1}^{\text{trial}} - 3G\Delta\lambda^{(k+1)^2})}{\rho_{n+1}c_v}$$
$$\bar{\sigma}_{n+1}^{(k+1)} = \bar{\sigma}_{n+1}^{(0)} - 3G\Delta\lambda^{(k+1)}$$
$$(k) \leftarrow (k+1)$$

After Convergence, stress is given by

$$\sigma_{\Re_{n+1}} = \sigma_{\Re_{n+1}}^{\text{trial}} - 3G\Delta\lambda\frac{s_{\Re_{n+1}}^{\text{trial}}}{\bar{\sigma}_{n+1}^{\text{trial}}} - 3\alpha K\Delta\theta 1$$

References

ABAQUS/Explicit v6.4 User's Manual, ABAQUS Inc., Richmond, USA, 2003.

Bäker, M., Rösler, J., Siemers, C., 2002. A finite element model of high speed metal cutting with adiabatic shearing. Computers and Structures 80 (5–6), 459–513.

Bodner, S.R., Partom, Y., 1975. Constitutive equations for elastic–viscoplastic strain-hardening materials. Journal of Applied Mechanics 42 (2), 385–389.

Doghri, I., 2000. Mechanics of Deformable Solids: Linear and Nonlinear, Analytical and Computational Aspects. Springer, Berlin (Chapter 16).

Duvaut, G., Lions, I.J., 1972. Les Inequations En Mechanique Et En Physique. Dunod, Paris.

Hagege, B., 2004. Simulation du comportement mécanique des renforts fibreux en grandes transformations: application aux renforts tricotés, Ph.D. thesis, ENSAM, Paris.

Heeres, O.M., 2001. Modern strategies for the numerical modelling of the cyclic and transient behaviour of soils, Ph.D. thesis, Tech. Univ. Delft.

Heeres, O.M., Suiker, A.S.J., de Borst, R., 2002. A comparison between the Perzyna viscoplastic model and the consistency viscoplastic model. European Journal of Mechanics A/Solids 21, 1–12.

Hodowany, J., Ravichandran, G., Rosakis, A.J., Rosakis, P., 2000. Partition of plastic work into heat and stored energy in metals. Experimental Mechanics 40, 113–123.

House, J.W., 1989. Taylor impact testing, Tech. Rep. AFATL-TR-89-41, Air Force Armament Laboratory, Eglin AFB, FL.

Johnson, G.R., Cook, W.H., 1983. A constitutive model and data for metals subjected to large strains, high strain rates, and temperatures. In: Proceedings of 7th International Symposium Ballistics. The Hague, The Netherlands, pp. 1–7.

Ju, J., 1990. Consistent tangent moduli for a class of viscoplasticity. Journal of Engineering Mechanics ASCE 116 (8), 1704–1779.

Khan, A.S., Huang, S., 1995. Continuum Theory of Plasticity. John Wiley & Sons, New York.

Lin, R.C., Brocks, W., 2004. On a finite strain viscoplastic theory base on a new internal dissipation inequality. International Journal of Plasticity 20, 1281–1311.

Litonski, J., 1977. Plastic flow of a tube under adiabatic torsion, Bulletin de L'Academie Polonaise Des Sciences, serie des Sciences Techniques XXV (7).

Meyers, M.A., 1994. Dynamic Behavior of Materials. Wiley, New York, p. 328.

Molinari, A., Musquar, C., Sutter, G., 2002. Adiabatic shear banding in high speed machining of Ti–6Al–4V: Experiments and modeling. International Journal of Plasticity 18 (4), 443–459.

Nagtegaal, J.C., 1982. On the implementation of inelastic constitutive equations with special reference to large deformation problems. Computer Methods in Applied Mechanics and Engineering 33, 469–484.

Nemat-Nasser, S., 1982. On finite deformation elastoplasticity. International Journal of Solids and Structures 18, 857–872.

Perzyna, P., 1966Fundamental Problems in Viscoplasticity, vol. 9. Academic Press, New York, pp. 243–377.

Ponthot, J.P., 2002. Unified stress update algorithms for the numerical simulation of large deformation elasto-plastic and elasto–viscoplastic processes. International Journal of Plasticity 18, 91–126.

Reyes, A., Langseth, M., Hopperstad, M., 2002. Crashworthiness of aluminum extrusions subjected to oblique loading: experiments and numerical analyses. International Journal of Mechanical Sciences 44 (9), 1965–1984.

Ristinmaa, M., Ottosen, N.S., 2000. Consequences of dynamic yield surface in viscoplasticity. International Journal of Solids and Structures 37, 4601–4622.

Rojek, J., Zinkiewicz, O.C., Oñate, E., Postek, E., 2001. Advanced in Fe explicit formulation for simulation of metal forming processes. Journal of Materials Processing Technology 119 (1–3), 41–47.

Rosenberg, Z., Dekel, E., 2004. On the role of material properties in the terminal ballistics of long rods. International Journal of Impact Engineering 30, 835–851.

Rule, W.K., 1997. A numerical scheme for extracting strength model coefficients form taylor test data. International Journal of Impact Engineering 19 (9–10), 797–810.

Rusinek, A., Klepaczko, J.R., 2001. Shear testing of a sheet steel at wide range of strain rates and a constitutive relation with strain-rate and temperature dependence of the flow stress. International Journal of Plasticity 17, 87–115.

Simo, J.C., Hughes, T.J.R., 1998. Computational Inelasticity. Springer, New York, Chapter 8.

Simo, J.C., Taylor, R.L., 1985. Consistent tangent operators for rate-independent elastoplasticity. Computer Methods in Applied Mechanics and Engineering 48, 101–118.

Wang, W.M., 1997. Stationary and propagative instabilities in metals. a computational point of view, Ph.D. thesis, Delft University of Technology.

Wang, W.M., Sluys, L.J., de Borst, R., 1997. Viscoplasticity for instabilities due to strain softening and strain-rate softening. International Journal of Numerical Methods in Engineering 40, 3839–3864.

Wilkins, M., 1964. Calculation of Elastoplastic Flows, vol. 3. Academic Press, pp. 211–263.

Winnicki, A., Pearce, C.J., Bićanić, N., 2001. Viscoplastic Hoffman consistency model for concrete. Computers and Structures 79, 7–19.

Yadav, S., Repetto, E.A., Ravichandran, G., Ortiz, M., 2001. A computational study of the influence of thermal softening on ballistic penetration in metals. International Journal of Impact Engineering 25, 787–803.

Zerilli, F.J., Armstrong, R.W., 1987. Dislocation-mechanics based constitutive relations for material dynamic calculations. Journal of Applied Physics 61 (5), 1816–1825.